Quaternion-based Signal Processing

Ben Witten and Jeff Shragge

ABSTRACT

Hypercomlex numbers, which have primarily been used for pattern recognition, offer many useful applications to geophysics. Image disparity estimation is a hypercomplex, phase-based technique, using quaternions, that can find differences between subtlety varying images. This technique relies on applying a quaternionic Fourier transform, a quaternionic Gabor filter and exploits the symmetries inherent in the quaternion. Two applications of hypercomplex image disparity estimation are time lapse analysis and boundary detection.

INTRODUCTION

Hypercomplex numbers are multi-dimensional numbers which have more than one complex plane. The most common type of hypercomplex numbers have 3 complex dimensions and one real one. These were introduced by Hamilton (1866) and he termed them quaternions. The most common application of quaternions has been towards Maxwell's equations. Recently, however, quaternions have been applied to signal processing, most notably pattern recognition. They have been useful for color image analysis where previous techniques have failed. This is because each complex quaternion axis can be associated with an RGB axis (Sanwine and Ell, 2000) which allows for color edge detection. In addition, they can be used for image segmentation, finding structure based not only upon color, but repeating patters. This has proven useful for finding defects in textiles (Bülow and Sommer, 2001). Another application is image disparity, which is used by Bülow (1999) to show how a pattern changes between two frames of a movie.

Image disparity offers many geophysical applications, as will be shown, because only organized structures, patterns, are detected by image disparity. Thus noise will have minimal effect. Since it is a phase based technique, even low amplitude signal still retain enough information to be viable for image disparity estimation. The applications that will be discussed here are time lapse analysis and edge detection.

To this end, the basics of hypercomplex mathematics will be shown, as will the quaternionic Fourier transform. Then the Gabor filter must be defined and extended to the quaternionic case. This will allow for the image disparity estimation to be calculated based upon multiple complex phases. Examples and applications to time lapse analysis and boundary detection with synthetics and real data are then shown.

HYPERCOMPLEX MATHEMATICS

The set of hypercomplex numbers is defined as

$$q = q_0 + \sum_{l=1}^{n} i_l q_l \quad q_l \in \Re.$$ (1)

Hypercomplex numbers define a n+1-dimensional complex space with i_l orthonormal to i_m, for $l \neq m$. For all cases presented in this paper l will be limited to 3. Such numbers are quaternions, which can be represented as $q = q_0 + i q_1 + j q_2 + k q_3$, where i, j, k are imaginary numbers that satisfying the following relations:

$$ij = -ji = k, \quad \text{and} \quad i^2 = j^2 = k^2 = -1.$$ (2)

The multiplication table for quaternion unit vectors is shown in Table 1.

Table 1: The multiplication table for quaternion algebra.

	1	i	j	k
1	1	i	j	k
i	i	-1	k	$-j$
j	j	$-k$	-1	i
k	k	j	$-i$	-1

With these definitions, quaternionic addition between two quaternions, q and p, can be defined as

$$\begin{aligned} q + p &= (q_0 + i q_1 + j q_2 + k q_3) + (p_0 + i p_1 + j p_2 + k p_3) \\ &= (q_0 + p_0) + i(q_1 + p_1) + j(q_2 + p_2) + k(q_3 + p_3), \end{aligned}$$ (3)

and multiplication as

$$\begin{aligned} qp &= (q_0 + i q_1 + j q_2 + k q_3)(p_0 + i p_1 + j p_2 + k p_3) \\ &= (q_0 p_0 - q_1 p_1 - q_2 p_2 - q_3 p_3) \\ &\quad + i(q_0 p_1 + q_1 p_0 + q_2 p_3 - q_3 p_2) \\ &\quad + j(q_0 p_2 + q_2 p_0 - q_1 p_3 + q_3 p_1) \\ &\quad + k(q_0 p_3 + q_3 p_0 + q_1 p_2 - q_2 p_1). \end{aligned}$$ (4)

Notice that multiplication in equation 4, is not commutative due to the quaternionic algebra rules defined in table 1. Quaternions are often separated into two parts, q_0 and $\mathbf{q} = i q_1 + j q_2 + k q_3$, respectively called the scalar and vector part of the quaternion. Using this definition, the conjugate of q, $\bar{q}$, is

$$\bar{q} = q_0 - \mathbf{q} = q_0 - i q_1 - j q_2 - k q_3$$ (5)

and the norm of a quaternion is defined by

$$\| q \| = \sqrt{q\bar{q}} = \sqrt{q_0{}^2 + q_1{}^2 + q_2{}^2 + q_3{}^2}. \tag{6}$$

It is useful to formulate a polar representation of the quaternion, as this will be the primary notation throughout this paper. For any complex number, $\mathbf{z} = a + ib$, the argument or phase-angle is defined as $\text{atan2}(b,a)$. If $\mathbf{z}$ is written it the form $\mathbf{z} = | r | e^{i\gamma}$, then γ is the phase (argument) of $\mathbf{z}$, denoted $\arg(\mathbf{z}) = \gamma$. Quaternions contain three complex subfields and, correspondingly, three phases that are the projections onto the i, j, or k-complex plane,

$$\phi = \arg_i(\mathbf{z}) = \text{atan2}(q_1, q_0) \tag{7}$$
$$\theta = \arg_j(\mathbf{z}) = \text{atan2}(q_2, q_0) \tag{8}$$
$$\psi = \arg_k(\mathbf{z}) = \text{atan2}(q_3, q_0). \tag{9}$$

Quaternionic Transform

Analogous to complex numbers, quaternions can be represented by a magnitude and three phases with

$$q = \| q \| e^{i\phi} e^{j\theta} e^{k\psi}. \tag{10}$$

Ell (1992) introduced the quaternionic Fourier transform (QFT) for two-dimensional signals,

$$F^q(\mathbf{u}) = \int_{R^2} e^{-i2\pi ux} f(\mathbf{x}) e^{-j2\pi vy} d^2\mathbf{x}, \tag{11}$$

where $\mathbf{x} = (x, y)^T$ and $\mathbf{u} = (u, v)^T \in R^2$ and f is a two-dimensional quaternion signal. Because two-dimensional signals can be decomposed into even and odd components along either the x- or y-axis, f can be written

$$f = f_{ee} + f_{oe} + f_{eo} + f_{oo},$$

with, for example, f_{oe} denoting the part of f that is odd with respect to x and even with respect to y. The QFT can now be decomposed to

$$\begin{aligned}
F^q(\mathbf{u}) = {} & \int_{R^2} cos(2\pi ux)cos(2\pi vy) f(\mathbf{x}) d^2\mathbf{x} \\
& -i \int_{R^2} \sin(2\pi ux)\cos(2\pi vy) f(\mathbf{x}) d^2\mathbf{x} \\
& -j \int_{R^2} \cos(2\pi ux)\sin(2\pi vy) f(\mathbf{x}) d^2\mathbf{x} \\
& +k \int_{R^2} \sin(2\pi ux)\sin(2\pi vy) f(\mathbf{x}) d^2\mathbf{x}.
\end{aligned} \tag{12}$$

The QFT is an invertible transform and most standard Fourier theorems hold for QFTs with minimal variation. These theorems will not be rederived here, as complete proofs of the QFT extension of Rayleigh's, the shift, the modulation, the derivative, and the convolution theorem exist elsewhere (Ell, 1992; Bülow, 1999).

QUATERNIONIC GABOR FILTERS

The three different types of signal phase, as described by Bülow (1999) are global, instantaneous, and local. Global phase is the angular phase of the complex Fourier transform of a signal. It gives a real-valued number for each point in the frequency domain that is indicative of the relative position of the frequency components. Instead of giving the phase of a certain frequency component, instantaneous and local phase give the phase at a certain position in a real signal. The instantaneous and local phases, however, do this in different ways. The instantaneous phase is the angular phase of the complex value at each signal position. The instantaneous phase has the drawback that while it provides local information, that information depends on the entire signal. This causes the instantaneous phase at any point to be effected by changes at any other point in the image, regardless of separation distance. To overcome this problem quadrature filters are employed. The local phase is defined as angular phase of the quadrature filter response at a particular position of the signal. In this paper, in order to obtain a local quaternion phase, quaterernonic Gabor filters are used. While quaternionic Gabor filters are not exact quaternonic quadrature filters, they are a good approximation to them.

Gabor filters are linear time-invariant (LTI) filters that exhibit many useful properties, which have led to their use in a wide range of signal processing applications. The impulse response of a two-dimensional Gabor filter is

$$h(x, y; u_0, v_0, \sigma, \epsilon) = g(x, y; \sigma, \epsilon)e^{i2\pi(u_0 x + v_0 y)} \tag{13}$$

where $g(x, y; \sigma)$ is the Gaussian with aspect ratio ϵ,

$$g(x, y; \sigma, \epsilon) = e^{-\frac{x^2 + (\epsilon y)^2}{\sigma^2}}. \tag{14}$$

Analogous to equation 13, a quaternionic Gabor filter is defined such that the impulse response to the filter is,

$$\begin{aligned} h^q(x, y; u_0, v_0, \sigma, \epsilon) &= g(x, y; \sigma, \epsilon)e^{i2\pi u_0 x}e^{j2\pi v_0 y} \\ &= g(x, y; \sigma, \epsilon)e^{i\omega_1 x}e^{j\omega_2 y} \end{aligned} \tag{15}$$

where $g(x, y; \sigma, \epsilon)$ is defined as in equation 14. The quaternionic Gabor filter can be split into its even and odd symmetries, just as the QFT and the original image. In that case the filter h can be written as

$$h^q(x, y; u_0, v_0, \sigma, \epsilon) = (h_{ee}^q + ih_{oe}^q + jh_{eo}^q + kh_{oo}^q). \tag{16}$$

Note that h_{ee}^q, h_{oe}^q, h_{eo}^q, and h_{oo}^q are real-valued functions (see Figure 1).

QUATERNIONIC DISPARITY ESTIMATION

Given two images, f_1 and f_2, it is possible to find a vector field, $\mathbf{d}(d_x, d_y)$, that relates the local displacement between f_1 and f_2 (i.e. $f_1(\mathbf{x}) = f_2(\mathbf{x} + \mathbf{d}(\mathbf{x}))$). Therefore, if the QFT of f_1 is,

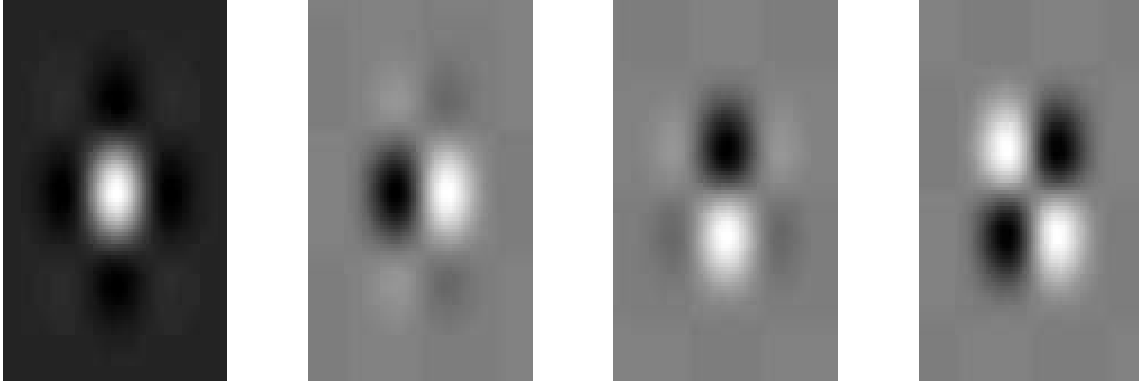$$f_1(x, y) \Longrightarrow F^q(u, v), \tag{17}$$

Figure 1: The h_{ee}, h_{oe}, h_{eo}, and h_{oo} symmetries of a quaternionic Gabor filter ben1-hs [CR]

then by the shift theorem,

$$f_2(x,y) = f_1(x+d_x, y+d_y) \Longrightarrow e^{i2\pi u d_x} F^q(u,v) e^{j2\pi u d_y}. \tag{18}$$

Knowing that f_1 and f_2 have local quaternionic phases $(\phi_1, \theta_1, \psi_1)$ and $(\phi_2, \theta_2, \psi_2)$ and assuming that ϕ varies only in x and θ varies only in y, then the displacement $\mathbf{d}(\mathbf{x})$ is given by

$$d_x(\mathbf{x}) = \frac{\phi_2(\mathbf{x}) - \phi_1(\mathbf{x})}{u_{ref}} \tag{19}$$

$$d_y(\mathbf{x}) = \frac{\theta_2(\mathbf{x}) - \theta_1(\mathbf{x})}{v_{ref}}. \tag{20}$$

The accuracy of the displacement depends strongly on the choice of the reference frequencies, u_{ref} and v_{ref}. The local model approach for quaternions outlined by Bülow (1999) will be used. This model assumes that the local phase at corresponding points of the two images will not differ, $\Omega_1(x,y) = \Omega_2(x+d_x, y+d_y)$, where $\Omega = (\phi, \theta)$. An estimate for $\mathbf{d}$ is obtained by a first-order Taylor expansion of Ω about x

$$\Omega_2(\mathbf{x}+\mathbf{d}) \approx \Omega_2(\mathbf{x}) + (\mathbf{d} \cdot \nabla)\Omega_2(\mathbf{x}). \tag{21}$$

Solving for $\mathbf{d}$ in equation 21 gives the disparity estimate for the local model. The disparity is estimated using equation 19 and the reference frequencies given by,

$$u_{ref} = \frac{\partial \phi_1}{\partial x}(\mathbf{x}), \quad v_{ref} = \frac{\partial \theta_1}{\partial y}(\mathbf{y}). \tag{22}$$

The local quaternionic phase components for anywhere in an image are given by

$$\phi(\mathbf{x}) = \frac{\text{atan2}(n_\phi(\mathbf{x}), d_\phi(\mathbf{x}))}{2}, \tag{23}$$

$$\theta(\mathbf{x}) = \frac{\text{atan2}(n_\theta(\mathbf{x}), d_\theta(\mathbf{x}))}{2}, \tag{24}$$

where n and d are related to the rotation matrix of a quaternion and are,

$$n_\phi = -2(k_{eo}^q(\mathbf{x})k_{oo}^q(\mathbf{x}) + k_{ee}^q(\mathbf{x})k_{oe}^q(\mathbf{x})), \tag{25}$$

$$d_\phi = (k_{ee}^q(\mathbf{x}))^2 - (k_{oe}^q(\mathbf{x}))^2 + (k_{eo}^q(\mathbf{x}))^2 - (k_{oo}^q(\mathbf{x}))^2, \tag{26}$$

$$n_\theta = -2(k_{oe}^q(\mathbf{x})k_{oo}^q(\mathbf{x}) + k_{ee}^q(\mathbf{x})k_{eo}^q(\mathbf{x})), \tag{27}$$

$$d_\theta = (k_{ee}^q(\mathbf{x}))^2 + (k_{oe}^q(\mathbf{x}))^2 - (k_{eo}^q(\mathbf{x}))^2 - (k_{oo}^q(\mathbf{x}))^2. \tag{28}$$

The k-functions are the responses of a symmetric component of the quaternionic Gabor filter to the image (e.g. $k_{ee}=(h_{ee} * f)(\mathbf{x})$). From equations 23 and 24 the derivatives of the local phase components are computed

$$\frac{\partial}{\partial x}\phi(\mathbf{x}) = \frac{d_\phi(\mathbf{x})\frac{\partial}{\partial x}n_\phi(\mathbf{x}) - n_\phi(\mathbf{x})\frac{\partial}{\partial x}d_\phi(\mathbf{x})}{n_\phi^2(\mathbf{x}) + d_\phi^2(\mathbf{x})}, \tag{29}$$

$$\frac{\partial}{\partial y}\theta(\mathbf{x}) = \frac{d_\theta(\mathbf{x})\frac{\partial}{\partial y}n_\theta(\mathbf{x}) - n_\theta(\mathbf{x})\frac{\partial}{\partial y}d_\theta(\mathbf{x})}{n_\theta^2(\mathbf{x}) + d_\theta^2(\mathbf{x})} \ . \tag{30}$$

Therefore, the disparity depends on the rate of change of the local phase as approximated by the quaternionic Gabor filters.

SYNTHETIC EXAMPLES

Figure 2 shows an instructive example with a shifted rectangular block. The upper left panel is the original block position while the upper right panel shows the same block shifted down and to the right by one point. On the bottom, the disparity is shown as both a magnitude and vector plot of the shift.   Figure 3 is similar to figure 2 except that, in addition to the larger rectangle, a smaller rectangle has appeared. If the disparity estimate were to run in the "forward" direction, then this block would be invisible. This is because it is based upon the derivative of the local phase of the left panel where the small block does not appear. In the "reverse" direction, however, the small block shows up. To remedy this, a pseudo-average is taken,

$$\mathbf{d}(\mathbf{x}) = (\mathbf{d}_f(\mathbf{x}) - \mathbf{d}_r(\mathbf{x}))/2, \tag{31}$$

where $\mathbf{d}_f(\mathbf{x})$ and $\mathbf{d}_r(\mathbf{x})$ are the disparities in the forward and reverse directions, respectively. The minus sign reverses the direction of the second disparity model to bring it into accordance with the first. Note that the block has no coherent direction as shown in the enlargement in figure 3. This should not be surprising since there is no sense of direction for something that materializes from nowhere. This technique of pseudo-averaging the forward and reverse disparities, however, has pitfalls. The image resulting from a single disparity estimate depends on the location of the original image. If the disparity between the images is too large, the forward and reverse will not coincide properly causing a "shadow" effect.

A map of the world is shown in figure 4. This image was subsequently shifted one percent to the west and two percent to the south. A clear disparity is shown on the bottom panel of
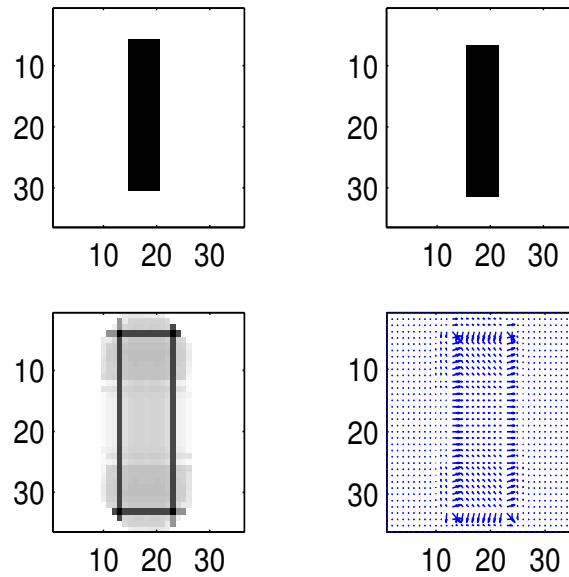
Figure 2: Top row: the input images. Bottom row: The disparity as a magnitude and a vector representation of disparity ben1-block1 [CR]
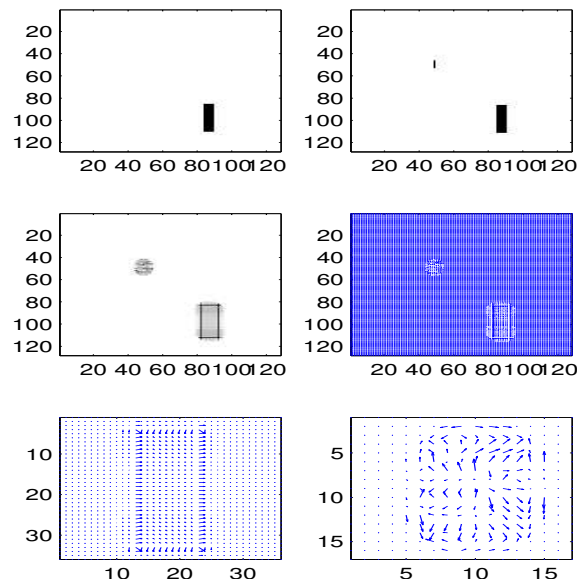

Figure 3: Top row: Images to be compared. Notice the appearance of the small block. Middle row: The magnitude and vector representations of the disparity using the pseudo-average. Bottom row: Zoomed image of the large block's and small block's, respectively, disparity in vector representation. ben1-block2 [CR]

figure 4. In figure 5, the same image is shown. The shift, however, is 15 percent to the east and 30 percent to the north. The shadow caused by the pseudo-average is clearly visible. There are two disparities that are equal but vary in position based upon where their respective image 1's were located. This pseudo-average has advantages, but for the purposes of this paper only the forward will be used from this point forward.
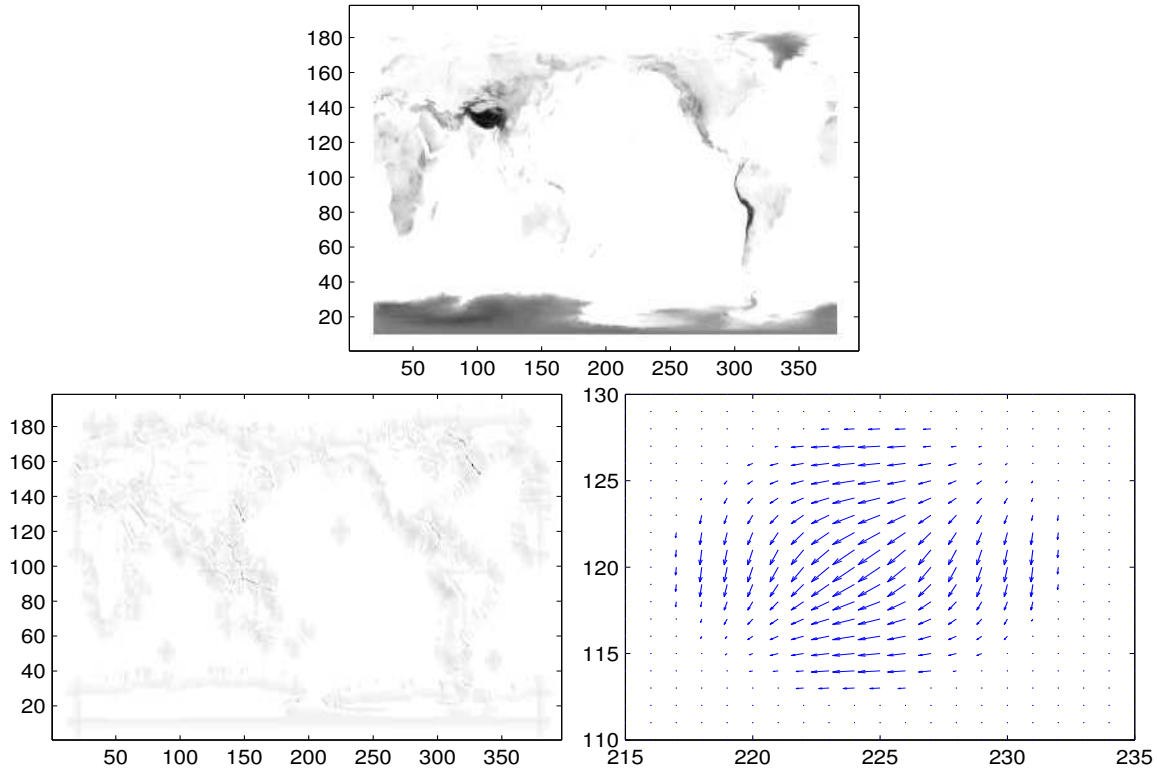

Figure 4: Top row: A map of the world. This image has been shifted one percent to the west and two percent to the south.Bottom row: the magnitude of the shift and a vector plot of the shift of the Big Island of Hawaii. ben1-world [CR]

APPLICATIONS

Time Lapse

One application for this procedure is assessing the temporal variation of time-lapse images. When seismic data are acquired in the same location at different times, disparity estimation can be used to visualize changes in the subsurface caused by compaction or fluid flow. This was done with three migrated images from the Duri Field in Indonesia that were collected over a 20 month period in the Duri Field of Indonesia. The original images (Lumley, 1995) are shown in figure 6 with the magnitude of the disparity between the images. The magnitude of the disparity offers very little information for this application. The vector representation, displayed in figure 7 with each vector scaled by 2, however, better accentuates the change
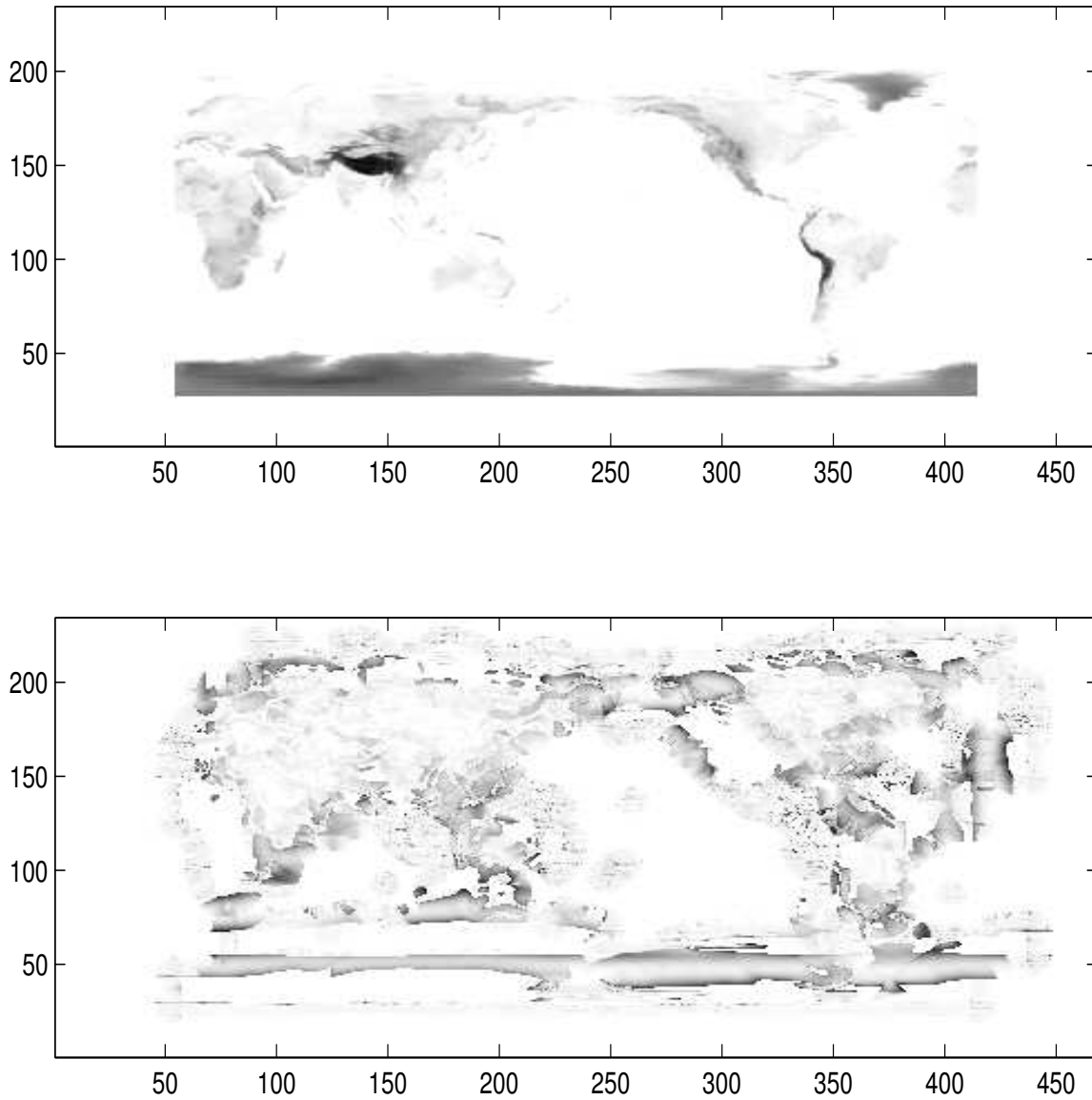
Figure 5: Top row: a map of the world. This will be shifted 15 percent to the east and 30 percent to the north. Bottom: The shadow effect caused by applying the pseudo-average for a large shift. Notice that there appears to be two disparity images varying only by a shift. ben1-world1 [CR]

providing useful information. Although it is hard to distinguish by looking at the migrated images, there are subtle changes that can be seen. The left edge of the hump near the center of the image increases slope from the left panel of figure 6 to the right. This slight change is detected by the image disparity algorithm and can be seen with downward pointing arrows near that have been circled in figure 7, corresponding to the left slope of the hump. This may be related to the insertion of an observation well near that location. The arrows do distinguish changes throughout the image, but it is very difficult to tell if these correspond to real changes, noise, or some slight variation caused by a change in acquisition.
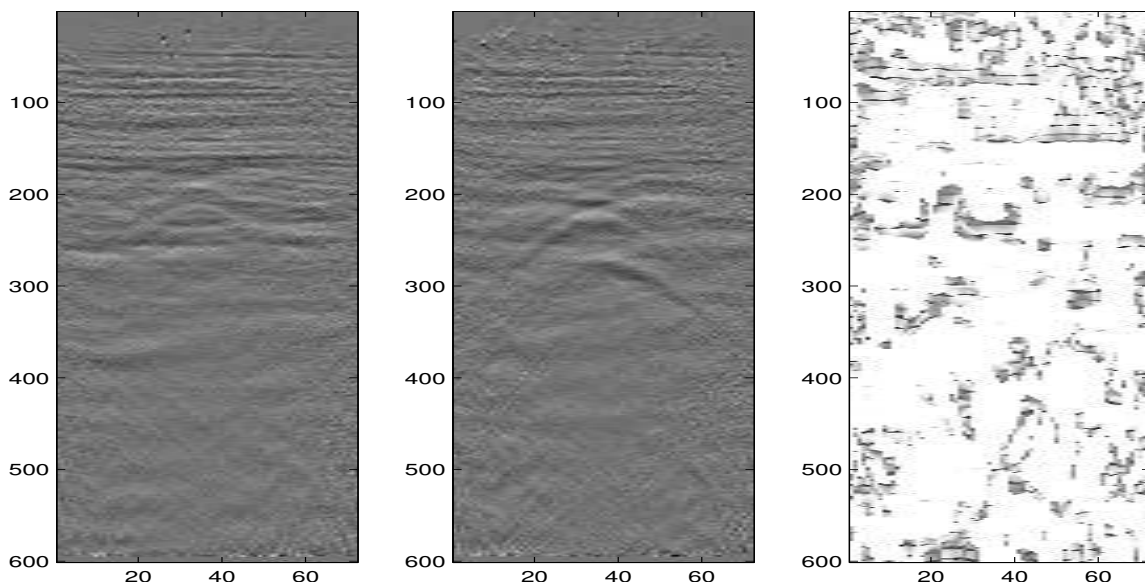

Figure 6: Two images from the same location at Duri Field at different times. Left:The magnitude of the change relative to the first image. ben1-lapse [CR]

Edge Detection

This procedure can also be used as an automated edge detection algorithm. This application can be accomplished by comparing a single image with a slightly shifted version of itself. When this is done the coherent structure is illuminated in the magnitude display of the disparity. Figure 8 shows the boundaries that have been detected using this algorithm for the first Duri image in figure 6. This method was also tested on a more complicated migrated data set that contains steeply dipping reflectors, from Tang and Clapp (2006). The result is shown in figure 9. It is encouraging even though this method fails to distinguish all of the layer boundaries that are clearly seen at the top of the original image. Although not demonstrated here, it is possible to shift only in the x-direction to highlight the vertical edges or shift in the y-direction to accentuate the horizontal edges. The sum of these two shifts will yield the same result as a single diagonal shift as done for these examples.
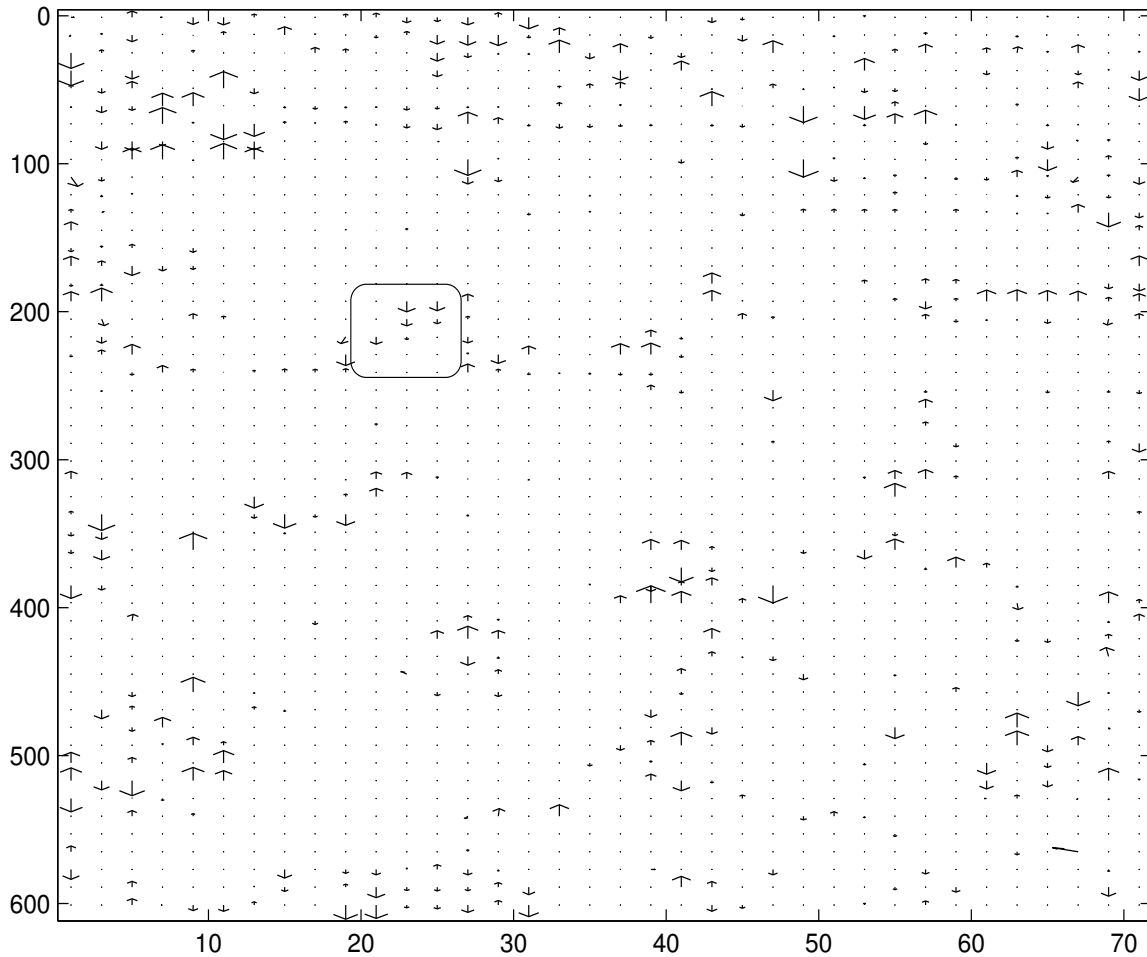
Figure 7: The disparity as a vector plot, sub-sampled by 2 in the x direction and 12 in the y direction. ben1-veclapse [NR]
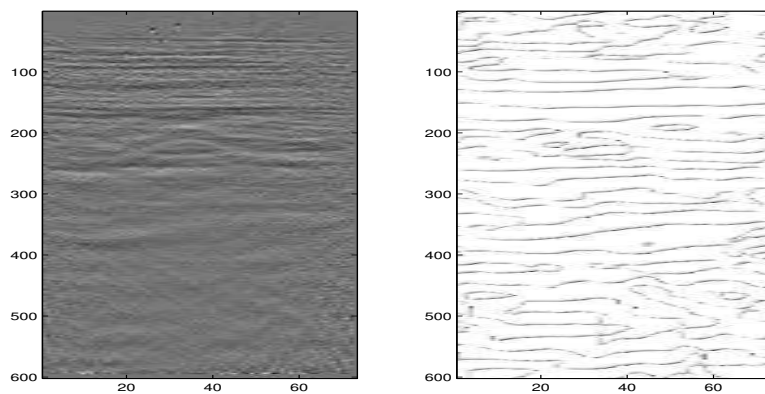

Figure 8: The original image and the boundaries found by image disparity with itself. ben1-edge1 [CR]
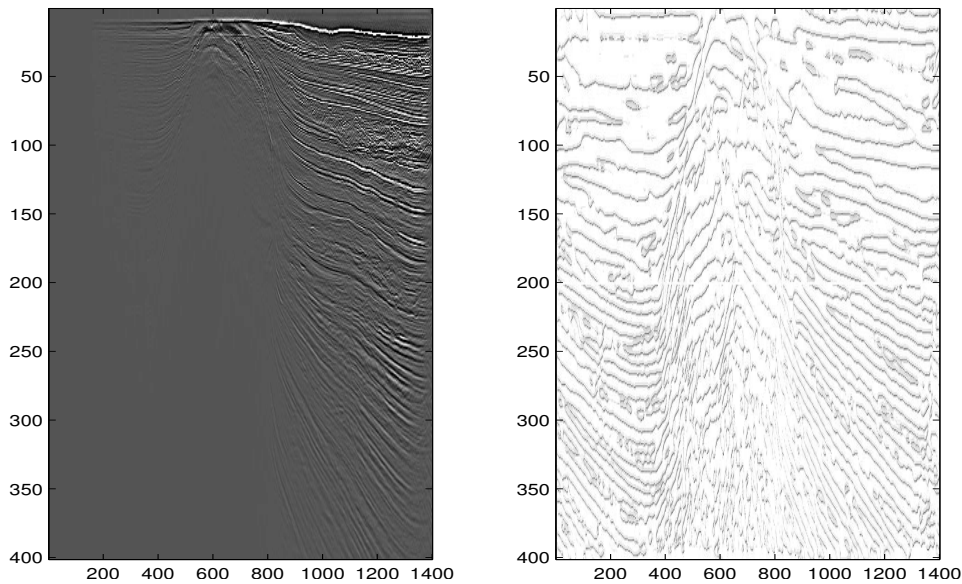
Figure 9: The original image and boundaries found by image disparity with itself. ben1-edge2 [CR]

CONCLUSION

Hypercomplex methods in general, and quaternionic in particular, offer numerous and diverse possibilities for geophysical purposes. This method is easy to implement and runs quickly and is efficient for time lapse analysis. Although the edge detection application does a reasonable job, it has not been as effective for shallow features as expected. The time lapse analysis offers an innovative way to quantitatively evaluated changes over time. As well, image disparity estimation has, thus far, have been unsuccessful on raw data. It was hoped to find boundaries or real of data and create an envelope to help remove noise. In future works, this technique may be extended to three dimensions or applied to other applications such as velocity model comparisons.

REFERENCES

Bülow, T. and G. Sommer, 2001, Hypercomplex signals: A novel extension of the analytic signal to the multidimensional case: IEEE Transactions on Signal Processing, **49**, 2844–2852.

Bülow, T., 1999, Hyercomplex spectral signal representations fro the processing and analysis of images: Inst. Comput. Sci. Appl. Math., Christian-Albrechts-Univ. Kiel, Kiel, Germany.

Ell, T., 1992, Hypercomplex spectral transformations: PhD thesis, Univ. Minnesota.

Hamilton, W., 1866, Elements of quaternions: Longmans Green, London.

Lumley, D., 1995, Seismic time-lapse monitoring of subsurface fluid flow: PhD thesis, Stanford University.

Sanwine, S. and T. Ell, 2000, Colour image filters based on hypercomplex convolution: Colour image filters based on hypercomplex convolution:, IEEE Proceedings- Vision, Image and Signal Processing, 89–93.

Tang, Y. and R. G. Clapp, 2006, Lloyd's algorithm for selecting reference anisotropic parameters during wavefield extrapolation: SEP–**124**.